# Dynamic Power Management System Employing a Single-Stage Power Converter for Standalone Solar PV Applications

Anand I, Subramaniam Senthilkumar, *Member, IEEE*, Dipankar Biswas, and M. Kaliamoorthy

***Abstract*—This paper presents a dynamic power flow management system for a solar photovoltaic (PV) system employing a single-stage single-inductor-based dual-input/output dc–dc converter feeding standalone dc loads backed up by a rechargeable battery. A time-sharing voltage-mode control scheme has been proposed for power flow management between solar PV, a battery, and a standalone dc load, and it also maintains a constant dc load voltage and performs maximum power point tracking operation of solar PV. The implementation of the control scheme has been described in detail. The steady-state performance of the single-stage converter has been explained with the relevant analytical expressions derived along with the characteristics. A state-space average model was developed for simulating the transient behavior and validating the working of the system for step changes in the input solar PV power and the dc loads. A hardware prototype of the proposed system has been fabricated, and the proposed controller has been implemented using the dSPACE DS1103 real-time interface board. The working of the proposed scheme for different levels of input solar insolation and dc load power demand has been satisfactorily demonstrated, and the corresponding results are also provided.**

***Index Terms*—Batteries, dc–dc power conversion, multiport circuits, photovoltaic (PV) power systems, power converter, solar power generation.**

## NOMENCLATURE

| | |
|---|---|
| $C_{\text{in}}$ | Input capacitance of the proposed converter, $\mu$F. |
| $C_o$ | Output capacitance of the proposed converter, $\mu$F. |
| $D_{D1}$ | Duty ratio of the diode $D_1$. |
| $D_{D\text{in}}$ | Duty ratio of the diode $D_{\text{in}}$. |
| $D_{S_{\text{boost}}}$ | Duty ratio of boost switch $S_{\text{boost}}$ of the proposed converter. |
| $D_{S2}$ | Duty ratio of the diode $S_2$. |
| $D_{S3}$ | Duty ratio of switch $S_3$. |
| $D_{D\text{in}}$ | Duty ratio of the input diode of the proposed converter. |
| $P_{\text{load}}$ | Standalone dc load power, W. |
| $P_{\text{pv}}$ | Solar PV power output, W. |
| $V_{\text{mpp}}$ | Voltage of the solar PV module at the maximum power point, V. |
| $V_{\text{bat}}$ | Terminal voltage of the battery, V. |
| $V_o^*$ | Reference voltage of the standalone dc load, V. |

Manuscript received December 15, 2017; accepted January 26, 2018. Date of publication February 9, 2018; date of current version September 28, 2018. Recommended for publication by Associate Editor C. A. Canesin. *(Corresponding author: Subramaniam Senthilkumar.)*

A. I and S. Senthilkumar are with the National Institute of Technology, Tiruchirappalli 620015, India (e-mail: anand.isaac@gmail.com; skumar@nitt.edu).

D. Biswas was with the National Institute of Technology, Tiruchirappalli 620015, India. He is now with Indian Oil Corporation Limited, New Delhi 110001, India (e-mail: dipankrbiswas1992@gmail.com).

M. Kaliamoorthy is with the Dr. Mahalingam College of Engineering and Technology, Pollachi 642003, India (e-mail: kaliasgoldmedal@gmail.com).

Color versions of one or more of the figures in this paper are available online at http://ieeexplore.ieee.org.

Digital Object Identifier 10.1109/TPEL.2018.2804658

## I. INTRODUCTION

HARNESSING renewable energy sources such as wind energy, solar energy, tidal energy, etc., is critical for overcoming problems due to global warming and environmental degradation caused by the use of fossil fuels. Among all renewable energy sources, solar photovoltaic (PV) is abundant, has high power density, and is modular and scalable. Solar PV is used in both grid-connected applications and standalone applications. It can be used in a wide range of applications from a microwatt Internet of Things system to a megawatt-scale solar PV plant [1], [2]. Solar PV operates in a wide range of dc voltages, while electrical and electronic systems also have different levels of dc voltage requirements [3]. Hence, it is necessary to use power electronic interfaces for solar PV applications.

Since the energy from solar PV is intermittent in nature, it is necessary to combine energy storage systems and other renewable energy sources to maintain a reliable operation for standalone PV systems. This can be achieved by many single-input/output (dual-port) dc–dc converters in parallel or multiport dc–dc converters. The centralized architecture of multiport converters uses fewer switches, has a compact structure, a lower cost, and a higher efficiency, and avoids the need to use communication systems as compared to multiple single-input/output dc–dc converters [4]–[6].

Sun *et al.* [4] have proposed a three-port converter incorporating solar PV and a battery as power sources feeding dc loads with galvanic isolation. The control structure involved a complex hybrid modulation technique (pulse width modulation (PWM) + pulse-frequency modulation) with soft switching. Ray *et al.* proposed an integrated dual-output dc–dc converter, which had both buck and boost outputs using PWM to regulate output voltages [7]. Various possible topologies for multiport converters have been discussed in [8]. However, using multiple inductors results in large converter size and cost. In order to overcome these problems, single-inductor multiple-input/output topologies have been proposed. Single-inductor multiple-output dc–dc converters based on buck, buck–boost, and boost topologies have been

proposed in various literature studies [9]–[13]. This reduces the cost and circuit complexity and results in greater efficiency.

Nami *et al.* [14] have proposed single-input multi-output boost converters based on the diode-clamped topology for multiple-series and multiple-parallel outputs using cascaded voltage and current control loops. Khaligh *et al.* [15] have proposed a single-inductor-based multi-input bidirectional dc–dc converter, which operates in buck, boost, and buck–boost modes. Various nonisolated single-inductor multi-input/output topologies have been reviewed in [16]. Isolated converters are used when there is a requirement for high step-up ratio and galvanic isolation. But the drawbacks are larger size and complexity compared to nonisolated converter topologies. Single-inductor multi-input multi-output topologies, which are a hybrid of multi-input multi-output converters, utilize multiple power sources to supply power to multiple applications [10], [17]–[20].

Bandyopadhyay and Chandrakasan [10] present a multi-input multi-output dc–dc converter utilizing three different power sources, namely piezoelectrics, solar PV, and thermoelectric for low-voltage applications. Huang and Chen [17] presented a multi-input multi-output dc–dc converter with buck and boost outputs for low-power portable applications using hysteresis and PWM control. Shao *et al.* [18] presented a dual-input/output dc–dc converter for low-power applications using solar PV as a power source and the battery as an energy storage device. Two modes of operation of the converter—the dual-input mode during deficit solar PV power and the dual-output mode during surplus solar PV power—are presented. Babaei and Abbasi [19] proposed a switched-capacitor-based boost converter topology, which is used for multiple outputs in series. A detailed analysis of the converter topology was carried out. Keyhani and Toliyat [20] proposed a zero-voltage-switching single-inductor multi-input multi-output converter with the buck–boost mode of operation.

This paper proposes a novel and simple time-sharing closed-loop control technique for the solar PV system with a single-inductor power converter stage, wherein the controller maintains a constant dc load voltage and a power flow management system to balance the power flow between solar PV, the battery, and standalone dc loads. The power converter is capable of operating in the dual-input/output mode controlled by an effective energy storage/energy management system for providing uninterrupted power supply to the standalone dc load from a battery to take care of both excess and deficit PV power availability situations. Steady-state analysis is performed by deriving analytical expressions and the transient analysis by developing a state-space average model of the proposed system. Starting with the description of the proposed system, steady-state analysis, the simulated and experimental waveforms of various electrical quantities are presented in the succeeding sections.

## II. Proposed Solar PV Power Flow Management System and Operation

The proposed system is shown in Fig. 1. It consists of a solar PV module as a power source, a battery as an energy storage element to supply during the absence of solar PV, a single-inductor-based dual-input/output dc–dc converter feeding a standalone dc load, and a controller that modulates power flow between a solar PV module, a battery, and a standalone dc load and performs voltage regulation at the standalone dc load terminals. The various functional blocks of the proposed system are as follows.

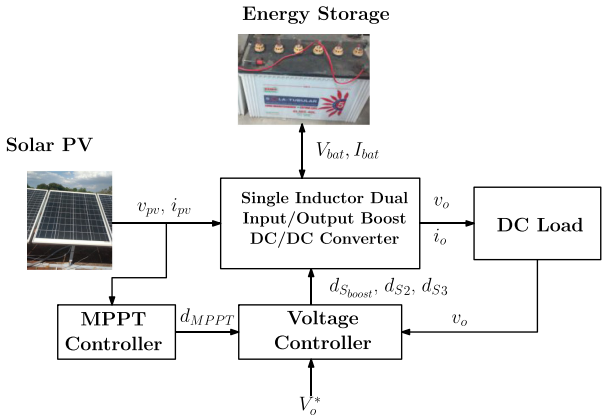


Fig. 1. Block diagram of the proposed power flow management system.

TABLE I
Parameters of the Solar PV Module at a Temperature of 25 °C

| | |
|---|---|
| Open-circuit voltage ($V_{oc}$) | 32.8 V |
| Short-circuit current ($I_{sc}$) | 2.6 A |
| Nominal voltage ($V_{mpp}$) | 24.65 V |
| Nominal current ($I_{mpp}$) | 2.44 A |
| Maximum power ($P_{mpp}$) | 60.3 W |

### A. Solar PV Module

The solar PV module is the primary source of power for the standalone dc load. The power generated by the solar PV module for a given temperature and level of irradiation depends on the PV voltage and current drawn by the load. Hence, in order to do load matching, a maximum power point tracking (MPPT) control is used to set the converter at the maximum power point (MPP) by varying the duty ratio of the appropriate switch and, hence, the current drawn by the converter from the solar PV module. There are many algorithms used to track the MPP, such as constant voltage, perturb and observe (P&O), incremental conductance, and the beta method [21]. Among them, a simple P&O algorithm is selected for the proposed system.

A 24-V 60-W solar PV module is selected for the proposed system, and the same is modeled using the five-parameter model [22]. The output current of the solar PV module used in modeling is

$$I_{\text{pv}} = I_L - I_o \left( e^{\frac{q(V + IR_s)}{nKT}} - 1 \right). \tag{1}$$

The key specifications of the solar PV module used are shown in Table I.

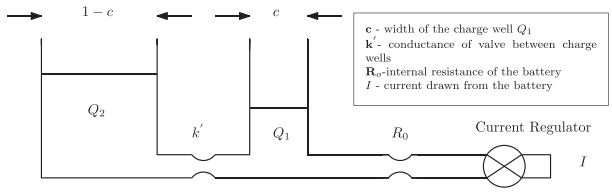


Fig. 2. Kinetic energy battery model.

### B. Energy Storage

Since the power from the solar PV module is intermittent, a rechargeable battery has to be used as an energy buffer to maintain the continuous operation of the system. During times of surplus PV power, it stores excess energy, and during times of deficit or absence of PV power, it complements or replaces the solar PV module as the power source. There are primarily two types of rechargeable batteries used for stationary power applications: the lead acid battery and the lithium ion battery. Since a lead acid battery is inexpensive and has less safety issues, it is used for the proposed system.

Jongerden and Haverkort have discussed various battery models [23]. For modeling the system, a kinetic battery model, an intuitive battery model based on electrical elements, is selected. The ampere hour capacity of lead acid batteries is rated for a particular duration of discharge—typically 10-h and 20-h rates of discharge. If the battery is discharged faster than the rated discharge, a lesser amount of capacity is available, and the battery has to be rested to recover the remaining charge. The kinetic battery takes this into account by modeling the lead acid battery into two charge wells: available charge with charge $Q_1$ and non-available charge $Q_2$, as shown in Fig. 2. The dynamic equations for the two charge wells are

$$\frac{dq_1}{dt} = -I + k^{'}\left(h_2 - h_1\right) \tag{2}$$

$$\frac{dq_2}{dt} = -k^{'}\left(h_2 - h_1\right). \tag{3}$$

The sum of the charges in the two charge wells gives the total remaining charge in the battery.

### C. Single-Inductor-Based Dual-Input/Output DC–DC Converter

The boost-derived single-inductor-based dual-input/output dc–dc converter used in the proposed power flow management system is shown in Fig. 3. It consists of the diode $D_{\text{in}}$, which interfaces the solar PV module to the converter and also prevents reverse power flow to the solar PV module. The capacitor $C_{\text{in}}$ is connected in parallel to the solar PV module to reduce the solar PV voltage ripples. Switch $S_2$ and diode $D_2$ are used to set the battery as an output to store excess solar PV power. Switch $S_3$ is used to set the battery as an input to supply power to the standalone dc load. The capacitor $C_o$ is connected across the output to reduce the output voltage ripples.

The converter has two modes of operation, namely the dual-output boost mode (DOBM) when the power from the solar PV module exceeds the dc load demand and the dual-input boost mode (DIBM) when there is a deficit. The circuit configuration for both the modes is shown in Fig. 4.

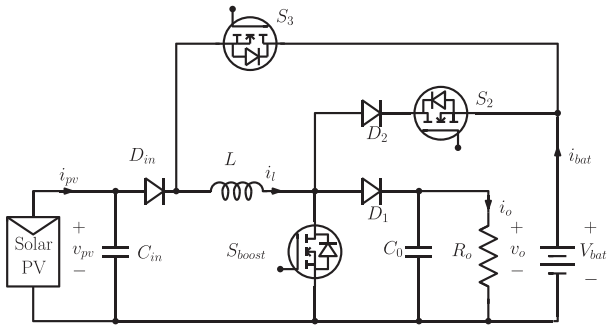


Fig. 3. Single-inductor-based dual-input/output boost dc–dc converter.

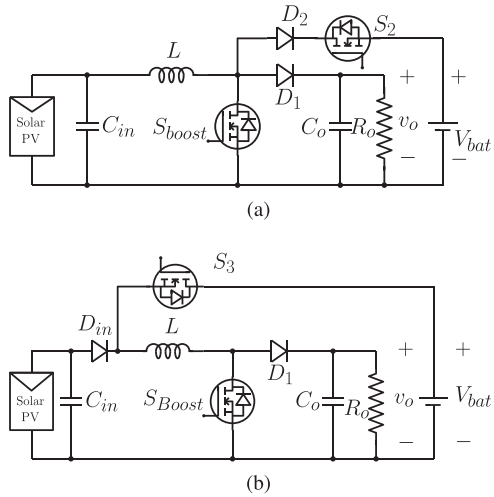


Fig. 4. Proposed single-inductor-based dual-input/output dc–dc converter in (a) DOBM and (b) DIBM.

During the DOBM, the solar PV module acts as a power source feeding the battery through switch $S_2$ and the dc load through diode $D_1$. The single-inductor-based dual-input/output dc–dc converter has three states, as shown in Fig. 5. In the first state, the inductor is charged by power from the solar PV module through switch $S_{\text{boost}}$. In the second state, switch $S_{\text{boost}}$ is turned OFF and the inductor discharges to the dc load through diode $D_1$. In the third state, the surplus power is discharged to the battery by turning ON switch $S_2$. Since the required voltage of the standalone dc load is higher than that of the battery, diode $D_1$ is reverse biased and the standalone dc load is cut off. Typical waveforms for the inductor current $i_l$, the inductor voltage $v_l$, the battery current $i_{\text{bat}}$, and the output dc load voltage $v_o$ for this mode are shown in Fig. 5.

By the volt–second principle, the output dc load voltage of the converter in the DOBM is obtained as

$$V_o = \frac{V_{\text{pv}} - V_{\text{bat}} D_{S2}}{D_{D1}}. \tag{4}$$

The equation is similar to the conventional boost converter equation, in which the effective input voltage is the difference between the solar PV module voltage $v_{\text{pv}}$ and the pulse modulated fraction of the battery voltage, $V_{\text{bat}} d_{S2}$. The variation of

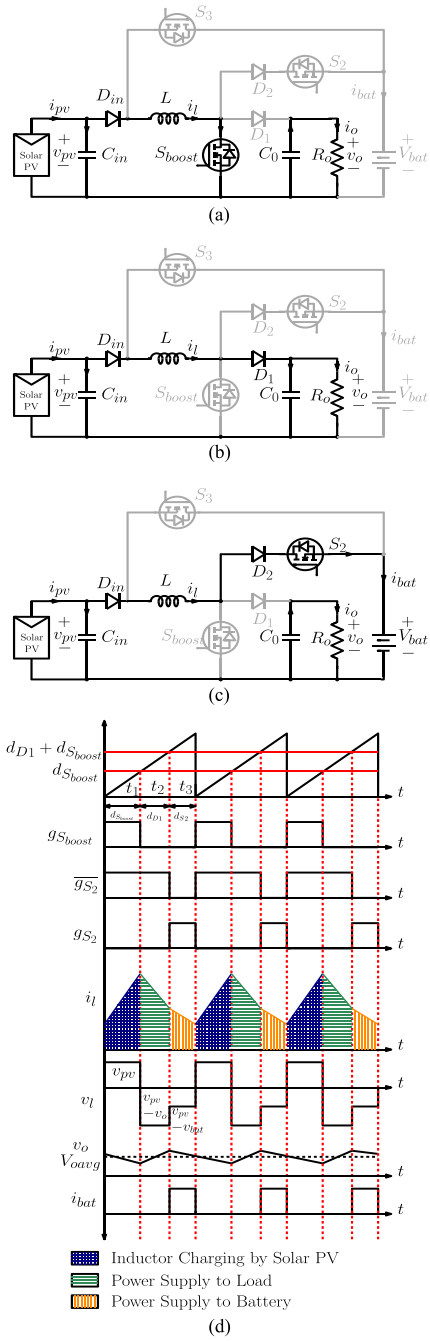


Fig. 5. Different circuit states in the DOBM. (a) Charging of the inductor by the solar PV module. (b) Discharge of the inductor to the standalone dc load. (c) Discharge of the inductor to the battery. (d) Typical waveforms during the DOBM.

the standalone dc load voltage with respect to the variation of duty cycles $d_{D1}$ and $d_{S2}$ for an input voltage of 24 V dc is observed in Fig. 6. It is seen that the standalone dc load voltage increases by either decreasing $d_{D1}$ or increasing $d_{S2}$. Rewriting (4), the required input voltage $V_{\text{pv}}$ for various duty ratios $d_{D1}$ and battery voltage $V_{\text{bat}}$ for an specific output voltage of $V_o$ can be calculated as

$$V_{\text{pv}} = V_o D_{D\text{in}} + V_{\text{bat}} D_{S2}. \tag{5}$$

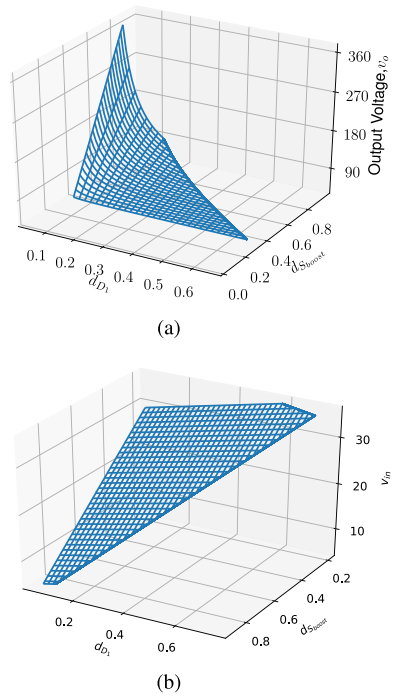


Fig. 6. Steady state Analysis in DOBM. (a) Output voltage variation with changes in $d_{S\text{boost}}$ and $d_{D\text{in}}$. (b) Required input PV voltage for an dc load voltage of 48 V for various duty ratios of $d_{D\text{in}}$ and $d_{S\text{boost}}$.

The required input voltage and duty ratios for a specific output voltage of 48 V dc and a battery voltage of 36 V dc is plotted in Fig. 6.

The converter has been modeled by using the state-space average model, developed by considering all the states of the circuit in the DOBM as follows:

$$\begin{bmatrix} \frac{di_l}{dt} \\ \frac{dv_{\text{pv}}}{dt} \\ \frac{dv_o}{dt} \end{bmatrix} = \begin{bmatrix} 0 & \frac{1}{L} & -\frac{d_{D1}}{L} \\ -\frac{1}{C_{\text{in}}} & 0 & 0 \\ \frac{d_{D1}}{C_o} & 0 & -\frac{1}{C_o R_o} \end{bmatrix} \begin{bmatrix} i_l \\ v_{\text{pv}} \\ v_o \end{bmatrix} + \begin{bmatrix} \frac{d_{S2}}{L} & 0 \\ 0 & \frac{1}{C_{\text{in}}} \\ 0 & 0 \end{bmatrix} \begin{bmatrix} V_{\text{bat}} \\ i_{\text{pv}} \end{bmatrix} \tag{6}$$

where $d_{D1}$ and $d_{S2}$ are duty ratios of diode $D_1$ and switch $S_2$, respectively.

In the DIBM, the battery and the solar PV module act as input power sources for the dc load. Switch $S_3$ sets the battery as an additional input power source. The single-inductor-based dual-input/output dc–dc converter has four circuit states, as shown in Fig. 7. In the first and second states, the inductor is charged by the solar PV module and the battery, respectively. The switch $S_{\text{boost}}$ is turned ON for both the states. Switch $S_3$ is turned ON for the second state to set the battery as the input power source. The diode $D_{\text{in}}$ is reverse biased as the battery voltage is more

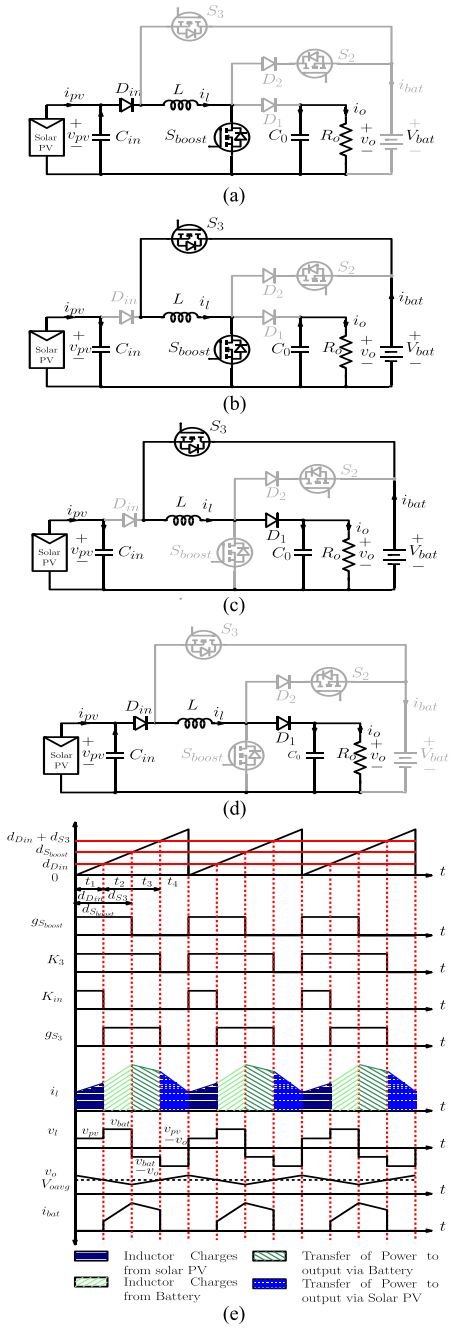


Fig. 7. Different circuit states in the DIBM. (a) Charging of the inductor by the solar PV module. (b) Charging of the inductor by the battery. (c) Discharge of the inductor to the dc load with the battery as a power source. (d) Discharge of the inductor to the output with the solar PV module as a power source. (e) Typical waveforms during the DIBM.

than the voltage of the solar PV module. During the third and fourth circuit states, switch $S_{\text{boost}}$ is turned OFF and the inductor discharges to the output. In the third circuit state, the battery is used as the power source by allowing switch $S_3$ to remain ON. During the fourth circuit state, switch $S_3$ is turned OFF and the solar PV module becomes the power source. Typical waveforms for the inductor current $i_l$, the inductor voltage $v_l$, the battery current $i_{\text{bat}}$, and the output voltage $v_o$ for this mode are shown in Fig. 7.

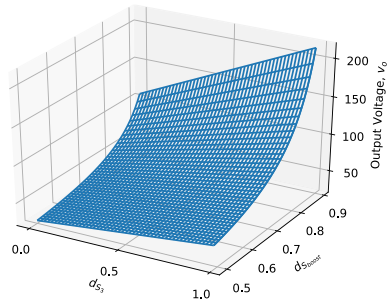


Fig. 8. Steady-state analysis in the DIBM—Variation of the output voltage for changes in $d_{S3}$ and $d_{S_{\text{boost}}}$ for $v_{\text{pv}} = 24$ V and $V_{\text{bat}} = 36$ V.

By the volt–second principle, the standalone dc load $V_o$ in the DIBM is found as

$$V_o = \frac{V_{\text{pv}} D_{D\text{in}} + V_{\text{bat}} \left(D_{S_{\text{boost}}} - D_{D\text{in}}\right)}{D_{S_{\text{boost}}}}. \tag{7}$$

It is observed that the relationship is similar to the conventional boost converter equation, in which the effective input voltage is the pulse modulated fraction of the input PV voltage and the battery voltage. The steady-state output voltage for a PV voltage of 24 V dc and a battery voltage of 36 V dc is plotted in Fig. 8. The 3-D plot shows that the output voltage increases linearly with increase in $d_{S3}$ and exponentially with increase in $d_{S_{\text{boost}}}$.

The state-space average model for the DIBM has been developed by considering all the circuit states as follows:

$$\begin{bmatrix} \frac{di_l}{dt} \\ \frac{dv_{pv}}{dt} \\ \frac{dv_o}{dt} \end{bmatrix} = \begin{bmatrix} 0 & \frac{\overline{d_{S3}}}{L} & -\frac{\overline{d_{S_{\text{boost}}}}}{L} \\ -\frac{\overline{d_{S3}}}{C_{\text{in}}} & 0 & 0 \\ \frac{\overline{d_{S_{\text{boost}}}}}{C_o} & 0 & 0 \end{bmatrix} \begin{bmatrix} i_l \\ v_{\text{pv}} \\ v_o \end{bmatrix} + \begin{bmatrix} \frac{d_{S3}}{L} & 0 \\ 0 & \frac{1}{C_{\text{in}}} \\ 0 & 0 \end{bmatrix} \begin{bmatrix} V_{\text{bat}} \\ i_{\text{pv}} \end{bmatrix} \tag{8}$$

where $d_{S_{\text{boost}}}$ and $d_{S3}$ are the duty ratios of switches $S_{\text{boost}}$ and $S_3$, respectively.

## III. Proposed Time-Sharing Control Strategy

The overall time-sharing control block diagram for the proposed power flow management system is shown in Fig. 9. It consists of a proportional–integral (PI) controller-based voltage regulator to regulate the standalone dc load voltage of 48 V. The reference voltage ($V_o^*$) and the actual standalone dc load voltage ($v_o$) are given to an error amplifier, which gives the absolute standalone dc load error voltage ($v_{oe}$), and it is then converted to a per-unit error voltage ($v_{oepu}$) by using the reference standalone dc load voltage as the base voltage. This per-unit error voltage is the input for the PI controller. The output of the voltage

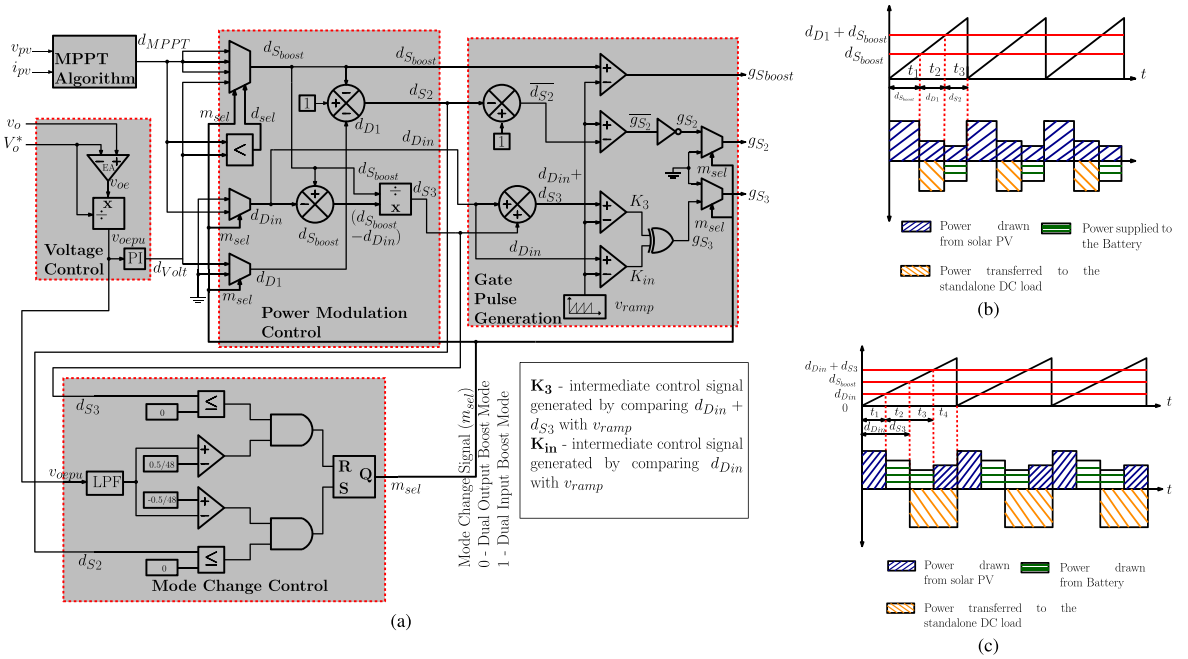


Fig. 9. Time-sharing control scheme for the proposed dynamic power flow management system. (a) Schematic diagram. (b) Power flow during the DOBM. (c) Power flow during the DIBM.

regulator ($d_{\text{Volt}}$) modulates the power flow for the dc load to address excess and deficit power based on the PV power availability by setting the appropriate mode of operation such as the DIBM and the DOBM. A simple P&O method is used for extracting the maximum power from the solar PV module by the control signal $d_{\text{MPPT}}$.

The mode change control decides the mode of operation of the converter by generating the mode signal $m_{\text{sel}}$ based on the standalone dc load power demand and the power extracted from the solar PV module. The rise in the standalone dc load voltage more than the standalone dc load reference voltage ($V_o^*$) shows that the power extracted from the solar PV is more than the load power demand and vice versa, which confirms the operation of the dual-output/input mode. The logic for the mode change signal is implemented by using logical and arithmetic operators. When the rise in the dc load voltage is 0.5 above $V_o^*$ and the duty ratio $d_{S3}$ is zero, the set-reset (SR) latch shown in the figure is reset to zero, which sets the converter in the DOBM. Similarly, when the fall in the dc load voltage is 0.5 below $V_o^*$ and the duty ratio $d_{S2}$ is zero, the SR latch is set to 1, which corresponds to the DIBM.

The power modulation control controls the appropriate switches to perform the operation of the power converter in the dual-input/output mode based on control signals $d_{\text{Volt}}$ and $d_{\text{MPPT}}$ and the mode signal $m_{\text{sel}}$ from mode change control by using arithmetic and logical operators. $m_{\text{sel}}$ acts as one of the selector signals for the multiplexers. In the DOBM, when there is excess solar PV power, MPPT is implemented by routing the MPPT control signal $d_{\text{MPPT}}$ to $d_{S_{\text{boost}}}$, and the voltage regulation of the standalone dc load is achieved by routing the voltage control signal $d_{\text{Volt}}$ to $d_{D1}$ by the multiplexers. The duty ratio $d_{S2}$ is created by subtracting a constant of 1 with $d_{S_{\text{boost}}}$ and $d_{D1}$. The sequence of duty ratios is shown in Fig. 5(d). The following expressions were implemented for the DOBM to operate power switches $S_{\text{boost}}$ and $S_2$:

$$d_{S_{\text{boost}}} = d_{\text{MPPT}} \tag{9}$$

$$d_{S2} = 1 - d_{D1} - d_{S_{\text{boost}}} \tag{10}$$

where

$$d_{D1} = d_{\text{Volt}}. \tag{11}$$

In the DIBM, when there is deficit solar PV power, both voltage regulation and MPPT control are achieved by the switch $d_{S_{\text{boost}}}$. The MPPT control signal $d_{\text{MPPT}}$ is routed to $d_{D\text{in}}$, and the voltage regulation of the standalone dc load is achieved by routing the voltage control signal $d_{\text{Volt}}$ to $d_{S_{\text{boost}}}$ through multiplexers. The sequence of duty ratios is shown in Fig. 7(e). The duty ratio $d_{S3}$ is obtained by subtracting $d_{S_{\text{boost}}}$ from $d_{D\text{in}}$ and then dividing by $d_{S_{\text{boost}}}$. When the solar PV power becomes surplus, the duty ratio $d_{S3}$ is slowly reduced to zero and the battery is cut off. This results in loss of MPPT as $d_{S_{\text{boost}}} = d_{D\text{in}} = d_{\text{Volt}}$. In order to regain control, the MPPT control signal $d_{\text{MPPT}}$ is routed to $d_{S_{\text{boost}}}$. A relational operator is used to detect this condition and generate the signal $d_{\text{sel}}$, which acts as a select signal for the multiplexer for $d_{S_{\text{boost}}}$. The following expressions were implemented for the power switches $S_{\text{boost}}$ and $S_3$ to operate the converter in the DIBM:

$$d_{S_{\text{boost}}} = d_{\text{Volt}} \tag{12}$$

$$d_{D\text{in}} = d_{\text{MPPT}} \leq d_{S_{\text{boost}}} \tag{13}$$

$$d_{S3} = \frac{d_{S_{\text{boost}}} - d_{D\text{in}}}{d_{S_{\text{boost}}}}. \tag{14}$$

From the outputs of the power modulation control ($d_{S_{\text{boost}}}$, $d_{S2}$, $d_{S3}$, and $d_{D\text{in}}$) and the mode change signal, the gating pulses

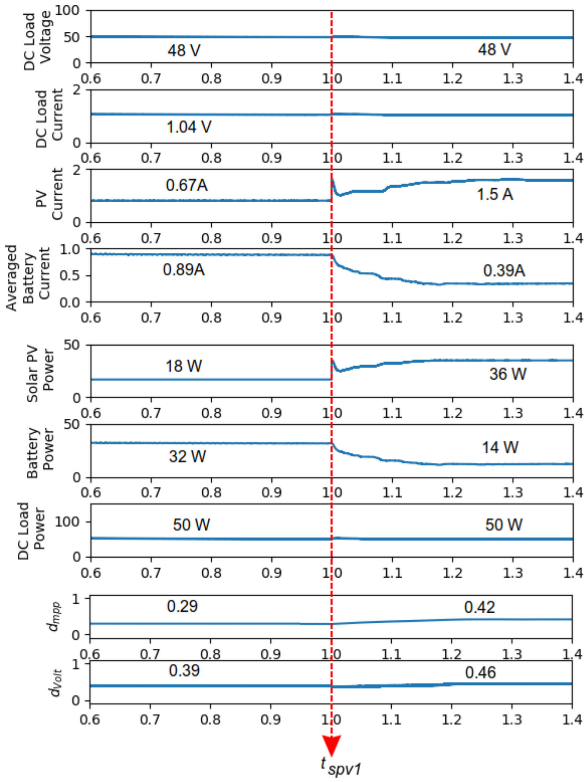


Fig. 10. Simulation of dynamic response of the converter to changes in PV power at $t_{\text{spv1}}$.

for the power switches $g_{S\,\text{boost}}$, $g_{S_2}$, and $g_{S_3}$ are generated using the gate pulse generation block. A ramp signal $v_{\text{ramp}}$ is used as a carrier signal for generating gate pulses. In the DIBM, to generate firing pulses for switches $S_{\text{boost}}$ and $S_3$ in the order as shown in Fig. 7, first, the duty ratio $d_{S_{\text{boost}}}$ is compared with $v_{\text{ramp}}$. Since the gate signal $g_{S_3}$ for switch $S_3$ has to be generated between time periods $t_1$ and $t_2$, it is generated in two steps. First, the two intermediate signals $K_3$ and $K_{\text{in}}$ are generated. Signal $K_3$ is generated by summing up $d_{D\,\text{in}}$ and $d_{S\,3}$ and comparing with $v_{\text{ramp}}$, and signal $K_{\text{in}}$ is generated by comparing $d_{D\,\text{in}}$ with $v_{\text{ramp}}$. Next, the intermediate signals $K_3$ and $K_{\text{in}}$ are XORed to get $g_{S_3}$. Similarly, for the DOBM, the gate signal $g_{S\,\text{boost}}$ is generated by comparing $d_{S_{\text{boost}}}$ with $v_{\text{ramp}}$.

The dc load voltage control, MPPT, and battery control are integrated by a time-sharing voltage mode control. Each control is allocated a time slot to perform power flow, as shown in Fig. 10. During the DOBM, as shown in Fig. 10(a), MPPT control decides the power drawn from the solar PV by controlling the switch $S_{\text{boost}}$ with the duty ratio $d_{\text{MPPT}}$. This occurs from time period 0 to $t_1$. The voltage controller regulates power flow to the load by determining the period of conduction of diode $D_1$ (from $t_1$ to $t_2$) by controlling the duty ratio $d_{\text{Volt}}$. The surplus power flow to the battery is indirectly regulated by the voltage controller by turning ON switch $S_2$ (from $t_2$ to $t_3$) for a duty ratio of $d_{S\,2}$. During the DIBM, as shown in Fig. 10(b), the voltage controller controls the power flow to the load by controlling switch $S_{\text{boost}}$ (from 0 to $t_2$) with a duty ratio of $d_{\text{Volt}}$. The MPPT control controls the power extracted from solar PV by determining the duration of conduction of diode $D_{\text{in}}$ (from 0 to $t_1$) for a duty ratio of $d_{\text{MPPT}}$. The deficit power is made up by the battery by making it as a power source for a duty ratio of $d_{S\,3}$ (from $t_1$ to $t_3$), which is determined by both the voltage controller and the MPPT controller according to (14).

## IV. Results and Discussion

### A. Simulation Results

The proposed power flow management system is simulated by implementing the state-space model derived in (8) in the MATLAB/Simulink environment. The values of the passive elements used are 100 $\mu$H for the boost inductor $L$ and 1000 $\mu$F for the input capacitor $C_{\text{in}}$ and the output capacitor $C_o$. A 60-W solar PV module with an MPP voltage of 24.5 V dc and an MPP current of 2.44 A and a battery with 36 V dc are used as power sources. The reference voltage of the standalone dc load is set at 48 V dc. The PI controller had values of $k_p = 5$ and $k_i = 15$ for per-unit error input.

*1) Case I: Increase in Solar Insolation From 300 to 600 W/m$^2$:* The power flow management system is initially operating in the DIBM with a solar PV insolation of 300 W/m$^2$, capable of supplying 18 W. The standalone dc load power demand is 50 W. The MPPT control maintains a $d_{\text{MPPT}}$ of 0.3 to extract 18 W from the solar PV module. The battery makes up for the power deficit of 32 W. At the time instant $t_{\text{spv1}}$ shown in Fig. 10, the solar insolation level is increased to 600 W/m$^2$, making the solar PV module capable of supplying a power of 36 W. The MPPT algorithm increases the duty ratio $d_{\text{MPPT}}$ to 0.4 to extract the maximum power. Since the effective input voltage $V_{\text{pv}} D_{D\,\text{in}} + V_{\text{bat}} (D_{S_{\text{boost}}} - D_{D\,\text{in}})$ shown in (7) decreases, the voltage controller increases the duty ratio $d_{\text{Volt}}$ to maintain the constant standalone dc load. Due to higher increase in $d_{\text{MPPT}}$ compared to $d_{\text{Volt}}$, $d_{S\,3}$ decreases in accordance with (13) and (14), and hence, the share of the battery power to the dc load power demand reduces to 14 W.

*2) Case II: Change in the Mode From DIBM to DOBM due to Surplus Power:* Initially, the power flow management system is operating at the DIBM with solar PV and battery supplying a load demand of 37 W. At the time instant $t_{lc}$, as shown in Fig. 11, the standalone dc load power demand is decreased to 12 W. The voltage controller decreases $d_{\text{Volt}}$ to regulate the standalone dc load voltage. When $d_{\text{Volt}}$ becomes less than $d_{\text{MPPT}}$, MPPT control is lost as $d_{D\,\text{in}}$ becomes less than $d_{\text{MPPT}}$. In this particular instant, the converter acts as a conventional boost converter with voltage control and the solar PV module as input. Hence, in order to further extract power from the solar PV module, the controller shifts to MPPT by setting $d_{S_{\text{boost}}}$ equal to $d_{\text{MPPT}}$. This results in loss of voltage control and rise of the load voltage above the reference voltage $V_o^*$. The mode change control shifts the converter to the DOBM almost immediately. The controller reduces the duty ratio $d_{D\,1}$ to reduce the standalone dc load voltage to $V_o^*$ and duty ratio $d_{S\,2}$ to divert excess power to batteries.

*3) Case III: Change in the Mode From DOBM to DIBM due to Deficit Power:* The power flow management system is initially operating at the DOBM with solar PV power of 36 W

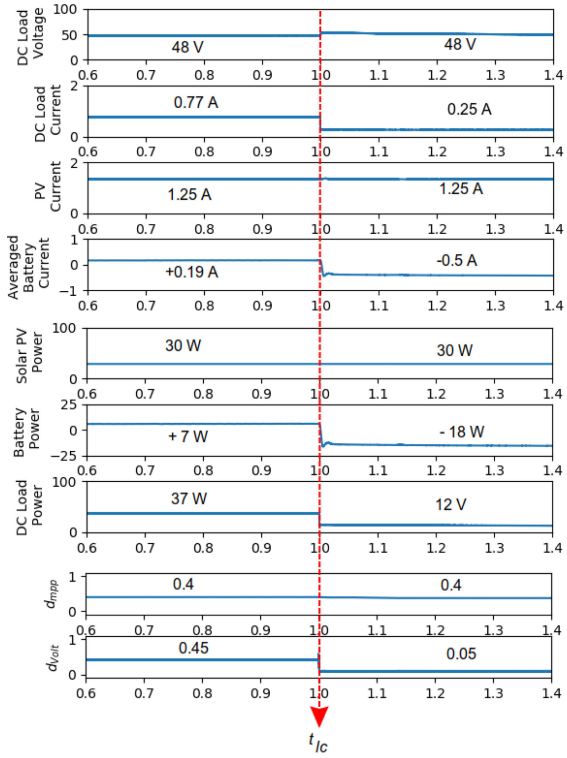


Fig. 11. Simulation of dynamic response of the converter to changes in the standalone dc load at $t_{lc}$.

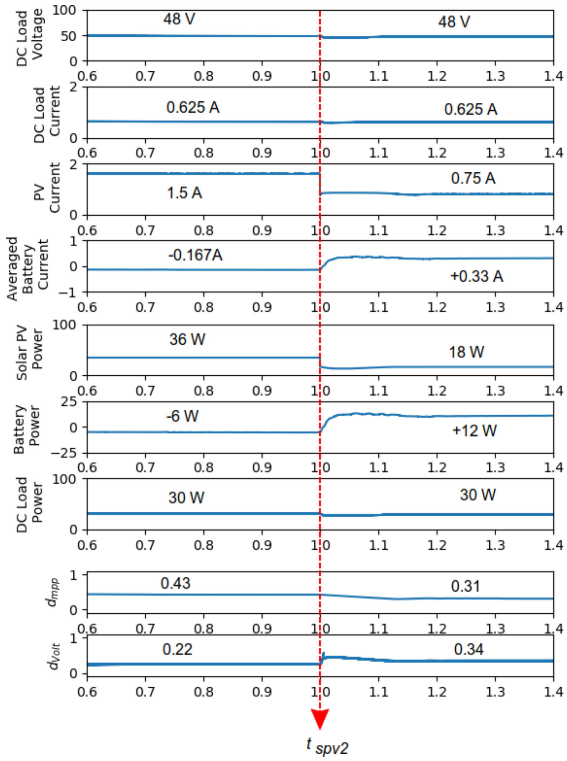


Fig. 12. Simulation of dynamic response of the converter to decrease in solar PV insolation at $t_{\text{spv2}}$.

(600 W/m$^2$). At the time instant $t_{\text{spv2}}$ shown in Fig. 12, the solar insolation level is decreased to 300 W/m$^2$, which results in power deficit. The MPPT algorithm adjusts the duty ratio $d_{\text{MPPT}}$ ($=d_{S_{\text{boost}}}$) to reach the new MPP. The deficit results in a decrease in $v_o$. The voltage controller compensates by increasing the duty ratio $d_{\text{Volt}}$ ($=d_{D\,1}$) to regulate the load voltage. This, in turn, results in a gradual decrease of the duty ratio $d_{S2}$ to zero and corresponding reduction of power flow to the battery to zero. At this point, voltage control is lost. This combined with the decrease in the dc load voltage $v_o$ below $V_o^*$ is used by the mode change control to shift the converter to the DIBM. In the DIBM, the voltage control signal $d_{\text{Volt}}$ is routed to $d_{S_{\text{boost}}}$, and it increases the voltage to $V_o^*$.

### B. Experimental Results

The single-inductor-based dual-input/output dc–dc converter in the power flow management system was fabricated by using MOSFET switches (IRF540N) rated at 23 A and 100 V and diodes (body diode of IRF540N) rated at 23 A. Three 24-V 60-W solar PV modules were used as power sources, and a resistive standalone dc load was used. A 36-V 40-Ah lead acid battery is used as energy storage. The input capacitor $C_{\text{in}}$ and the dc load capacitor $C_o$ were rated at 1000 $\mu$F. A 100-$\mu$H toroidal inductor rated at 20 A is used. The converter is switched at 100 kHz. The controller is implemented by using MATLAB/Simulink programming, and the generated code is dumped into the dSPACE DS1103 RTI board. The feedback is achieved by using LV 25-p voltage and LA 55-p current sensors. A passive low-pass

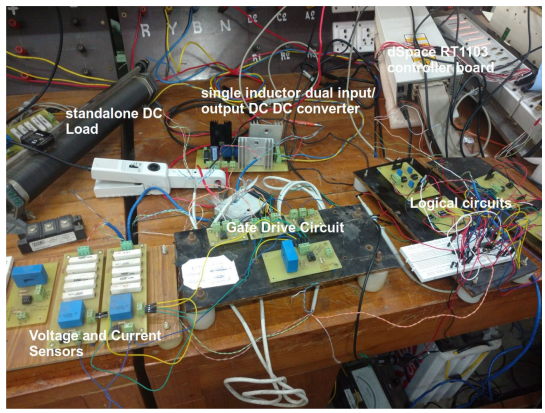


Fig. 13. Experimental setup of the power flow management system.

filter with a corner frequency of 1 kHz is used to eliminate noise in the feedback circuit. The PI controller parameters are $k_p = 0.5$ and $k_i = 8$. The power quantities $P_{\text{load}}$, $P_{\text{bat}}$, and $P_{\text{pv}}$ are computed inside the dSPACE DS1103 real-time interface (RTI) board and recorded in a digital storage oscilloscope (DSO). The gate pulses are generated by using the dSPACE DS1103 RTI board and the XOR logic gate. The gate pulses are then fed to LM339, a quad package comparator that acts as a buffer between the dSPACE DS1103 RTI board and HCPL-3120 optocouplers. The optocouplers are then interfaced with appropriate switches. The experimental setup is shown in Fig. 13.

*1) Case I: Dynamic Response of the Converter due to Increase in the Solar PV Input From 18 to 36 W:* The converter

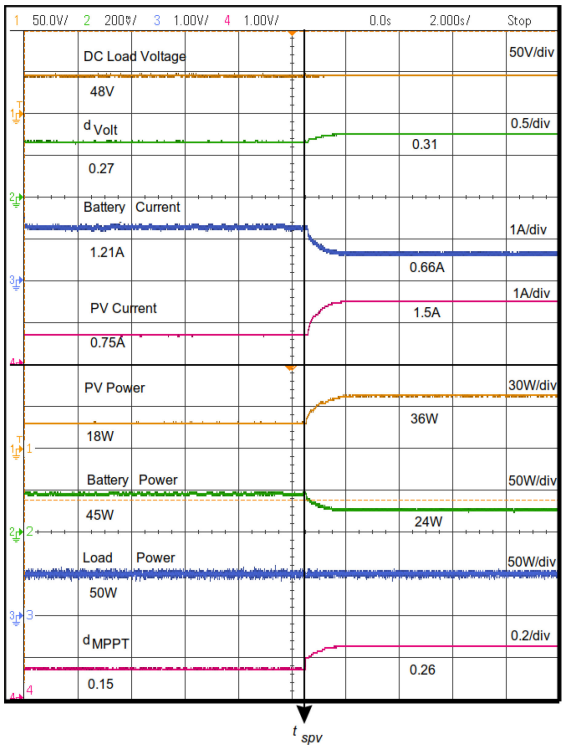


Fig. 14. Experimentation Case I: Dynamic response of the converter to changes in solar PV insolation.

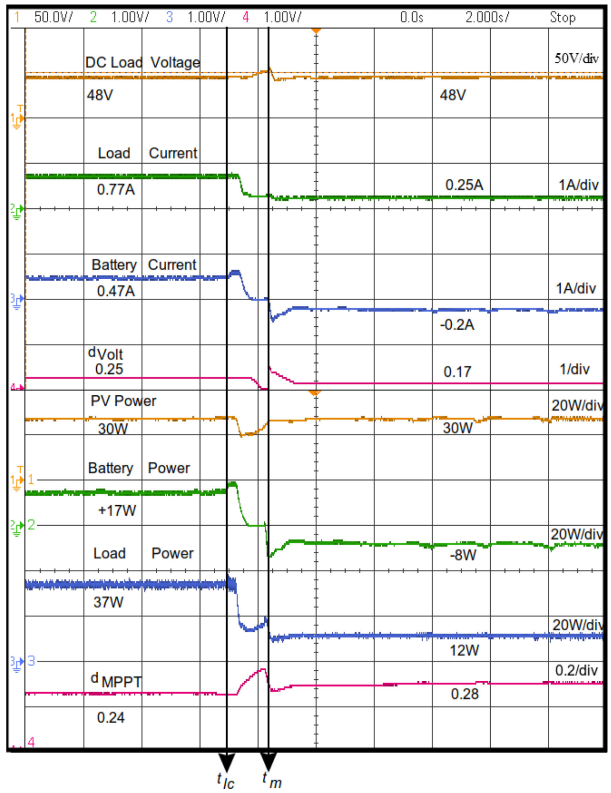


Fig. 15. Experimentation Case II: Dynamic response of the converter to changes in load.

is operating at the DIBM with both solar PV and the battery satisfying a standalone dc load demand of 50 W. At the time instant $t_{\text{spv}}$, as shown in Fig. 14, the solar PV input was doubled to 36 W. The MPPT controller increases $d_{\text{MPPT}}$ to shift the solar PV to the new MPP. The voltage controller increases $d_{\text{Volt}}$ as the effective input voltage, as shown in (7), is reduced due to increase in $d_{D\,\text{in}}$. Due to increase in $d_{D\,\text{in}}$ [see (13)], $d_{S3}$ [see (14)] decreases, and hence, the power drawn from the battery decreases.

*2) Case II: Mode Change to the DOBM due to Decrease in the Standalone DC Load From 37 to 12 W:* The standalone dc load power demand was 37 W, which is supplied by both solar PV and the battery with the converter in the DIBM. At the time instant $t_{lc}$, as shown in Fig. 15, the standalone dc load power demand is reduced to 12 W. Due to surplus power, the voltage increases. The voltage controller reduces $d_{\text{Volt}}$. After it reaches equal to $d_{\text{MPPT}}$, the MPPT control takes over control of switch $S_3$, which results in loss of voltage control. The mode change control then shifts the converter from the DIBM to the DOBM at time $t_m$ to divert surplus power to charge the battery bank. The voltage control is now restored, and the standalone dc load voltage is regulated to $V_o^*$.

*3) Case III: Mode Change to the DIBM due to Decrease in the Solar PV Input From 36 to 18 W:* The converter is operating at the DOBM with a standalone dc load power demand of 20 W and the solar PV input of 36 W. At the time instant $t_{\text{spv}}$, as shown in Fig. 16, the solar PV input is halved from 36 to 18 W. Since the standalone dc load power demand is 20 W, this results in deficit power and decrease in $v_o$. The MPPT control decreases

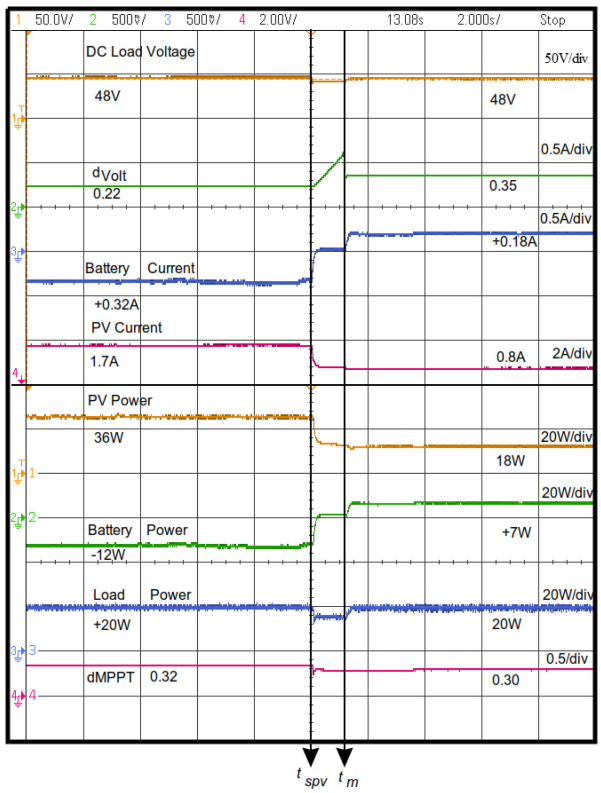


Fig. 16. Experimentation Case III: Dynamic response of the converter to changes in solar PV insolation.

TABLE II
OPERATION OF THE PROPOSED SYSTEM UNDER VARIOUS LEVELS OF SOLAR PV POWER AND OUTPUT DC LOAD DEMAND WITH A BATTERY VOLTAGE OF 36 V DC AND AN OUTPUT VOLTAGE OF 48 V DC

| Number of panels | $V_{\text{pv}}$ (V) | $I_{\text{pv}}$ (A) | $P_{\text{pv}}$ (W) | $V_{\text{bat}}$ (V) | $I_{\text{bat}}$ (A) | $P_{\text{bat}}$ (W) | $V_o$ (V) | $I_o$ (A) | $P_{\text{load}}$ (W) | Mode |
|---|---|---|---|---|---|---|---|---|---|---|
| 1 | 24 | 1.04 | 25 | 36.5 | 0.7 | 28 | 48 | 0.94 | 45 | DIB |
| 1 | 24.1 | 0.62 | 15 | 36.8 | 0.244 | 9 | 48 | 0.42 | 20 | DIB |
| 2 | 24.3 | 1.64 | 40 | 37.1 | −0.49 | −18 | 48 | 0.313 | 15 | DOB |
| 3 | 24.2 | 3.72 | 90 | 37.1 | −0.7 | −26 | 48 | 1.04 | 50 | DOB |
| 2 | 24.3 | 3.09 | 75 | 36.7 | 0.84 | 31 | 48 | 1.88 | 90 | DIB |

$d_{\text{MPPT}}$ to shift to the new MPP. The voltage controller increases $d_{\text{Volt}}$ to compensate for drop in $v_o$, but this is not enough. The mode change control shifts the converter from the DOBM to the DIBM at time $t_m$ to use the battery as an additional power source to make up for the power deficit. The voltage controller then regulates $d_{\text{Volt}}$ to bring $v_o$ to $V_o^*$.

The converter is also operated under several more levels of solar PV power and load demand, as shown in Table II. The different levels of solar PV power are obtained by changing the number of solar PV panels in parallel.

The simulation and experimental results prove the efficacy of the proposed power flow management system for standalone solar PV applications.

## V. CONCLUSION

A power flow management system for battery-backed standalone solar PV systems employing a single-stage single-inductor dual-input/output dc–dc converter has been presented. A novel time-sharing voltage-mode control scheme has been proposed for power flow management between solar PV, the battery, and dc loads to maintain a constant dc load voltage and also extract the maximum power from solar PV. The converter is capable of operating both in surplus and deficit PV power. A hardware prototype of the proposed system consisting of solar PV, the single-inductor-based dual-input/output dc–dc converter, and a battery bank has been fabricated, and the control circuits have been implemented on a dSPACE DS1103 RTI board.

The steady-state operation of both the DOBM and the DIBM has been simulated and validated using the MATLAB programming language, and the characteristics are presented. A state-space average model of the proposed system was developed to perform transient analysis of the system. Simulated waveforms of the PV current, the standalone dc load voltage, the standalone dc load current, the averaged battery current, the solar PV power, the battery power, and the standalone dc load power obtained using this model are shown for changes in levels of incident solar insolation and the dc load on the system. These dynamic changes were also carried out in the experimental setup, and the waveforms of the corresponding electrical quantities were captured in the DSO and are presented. The simulation and experimental performance presented confirms the satisfactory working of the controller in maintaining the desired dc load voltage under the varying operating conditions of solar PV insolation and consumer load.

## ACKNOWLEDGMENT

The authors would like to thank the authorities of the National Institute of Technology, Tiruchirappalli, India, for all the facilities provided for carrying out the experimental and simulation work at the Switched Mode Power Conversion Research Laboratory for the preparation of this paper.

## REFERENCES

[1] X. Liu and E. Snchez-Sinencio, "A highly efficient ultralow photovoltaic power harvesting system with MPPT for internet of things smart nodes," *IEEE Trans. Very Large Scale Integr. (VLSI) Syst.*, vol. 23, no. 12, pp. 3065–3075, Dec. 2015.

[2] M. Ito, K. Kato, H. Sugihara, T. Kichimi, J. Song, and K. Kurokawa, "A preliminary study on potential for very large-scale photovoltaic power generation (VLS-PV) system in the gobi desert from economic and environmental viewpoints," *Sol. Energy Mater. Sol. Cells*, vol. 75, nos. 3/4, pp. 507–517, 2003. [Online]. Available: http://www.sciencedirect.com/science/article/pii/S0927024802001988

[3] C. D. Xu and K. W. E. Cheng, "A survey of distributed power system—AC versus dc distributed power system," in *Proc. 4th Int. Conf. Power Electron. Syst. Appl.*, Jun. 2011, pp. 1–12.

[4] X. Sun, Y. Shen, W. Li, and H. Wu, "A PWM and PFM hybrid modulated three-port converter for a standalone PV/battery power system," *IEEE J. Emerg. Sel. Topics Power Electron.*, vol. 3, no. 4, pp. 984–1000, Dec. 2015.

[5] Y. C. Liu and Y. M. Chen, "A systematic approach to synthesizing multi-input dc-dc converters," *IEEE Trans. Power Electron.*, vol. 24, no. 1, pp. 116–127, Jan. 2009.

[6] Y. M. Chen, A. Q. Huang, and X. Yu, "A high step-up three-port dc-dc converter for stand-alone PV/battery power systems," *IEEE Trans. Power Electron.*, vol. 28, no. 11, pp. 5049–5062, Nov. 2013.

[7] O. Ray, A. P. Josyula, S. Mishra, and A. Joshi, "Integrated dual-output converter," *IEEE Trans. Ind. Electron.*, vol. 62, no. 1, pp. 371–382, Jan. 2015.

[8] H. Wu, J. Zhang, and Y. Xing, "A family of multiport buck-boost converters based on dc-link-inductors (DLIS)," *IEEE Trans. Power Electron.*, vol. 30, no. 2, pp. 735–746, Feb. 2015.

[9] W.-H. Ki and D. Ma, "Single-inductor multiple-output switching converters," in *Proc. IEEE 32nd Annu. Power Electron. Spec. Conf.*, 2001, vol. 1, pp. 226–231.

[10] S. Bandyopadhyay and A. P. Chandrakasan, "Platform architecture for solar, thermal, and vibration energy combining with MPPT and single inductor," *IEEE J. Solid-State Circuits*, vol. 47, no. 9, pp. 2199–2215, Sep. 2012.

[11] L. Benadero, V. Moreno-Font, R. Giral, and A. E. Aroudi, "Topologies and control of a class of single inductor multiple-output converters operating in continuous conduction mode," *IET Power Electron.*, vol. 4, no. 8, pp. 927–935, Sep. 2011.

[12] W. Jiang and B. Fahimi, "Multiport power electronic interface—Concept, modeling, and design," *IEEE Trans. Power Electron.*, vol. 26, no. 7, pp. 1890–1900, Jul. 2011.

[13] Y. J. Moon, Y. S. Roh, J. C. Gong, and C. Yoo, "Load-independent current control technique of a single-inductor multiple-output switching dc-dc converter," *IEEE Trans. Circuits Syst. II, Express Briefs*, vol. 59, no. 1, pp. 50–54, Jan. 2012.

[14] A. Nami, F. Zare, A. Ghosh, and F. Blaabjerg, "Multi-output dc-dc converters based on diode-clamped converters configuration: Topology and control strategy," *IET Power Electron.*, vol. 3, no. 2, pp. 197–208, Mar. 2010.

[15] A. Khaligh, J. Cao, and Y.-J. Lee, "A multiple-input DC–DC converter topology," *IEEE Trans. Power Electron.*, vol. 24, no. 3, pp. 862–868, Mar. 2009.
[16] Z. Rehman, I. Al-Bahadly, and S. Mukhopadhyay, "Multiinput dc–dc converters in renewable energy applications—An overview," *Renew. Sustain. Energy Rev.*, vol. 41, pp. 521–539, 2015.
[17] M. H. Huang and K. H. Chen, "Single-inductor multi-output (SIMO) DC-DC converters with high light-load efficiency and minimized cross-regulation for portable devices," *IEEE J. Solid-State Circuits*, vol. 44, no. 4, pp. 1099–1111, Apr. 2009.
[18] H. Shao, X. Li, C. Y. Tsui, and W. H. Ki, "A novel single-inductor dual-input dual-output dc-dc converter with PWM control for solar energy harvesting system," *IEEE Trans. Very Large Scale Integr. (VLSI) Syst.*, vol. 22, no. 8, pp. 1693–1704, Aug. 2014.
[19] E. Babaei and O. Abbasi, "Structure for multi-input multi-output dc-dc boost converter," *IET Power Electron.*, vol. 9, no. 1, pp. 9–19, 2016.
[20] H. Keyhani and H. A. Toliyat, "A ZVS single-inductor multi-input multi-output dc-dc converter with the step up/down capability," in *IEEE Energy Convers. Congr. Expo.*, Sep. 2013, pp. 5546–5552.
[21] M. A. G. de Brito, L. Galotto, L. P. Sampaio, G. d. A. e Melo, and C. A. Canesin, "Evaluation of the main MPPT techniques for photovoltaic applications," *IEEE Trans. Ind. Electron.*, vol. 60, no. 3, pp. 1156–1167, Mar. 2013.
[22] A. Luque and S. Hegedus, *Handbook of Photovoltaic Science and Engineering*. New York, NY, USA: Wiley, 2011.
[23] M. R. Jongerden and B. R. Haverkort, "Which battery model to use?" *IET Softw.*, vol. 3, no. 6, pp. 445–457, Dec. 2009.

**Anand I** received the Bachelor's degree in electrical and electronics engineering from the PSG College of Technology, Coimbatore, India, in 2009, and the Master's degree in power electronics from Sri Sivasubramaniya Nadar College of Engineering, Chennai, India, in 2013. He is currently working toward the Ph.D. degree at the National Institute of Technology, Tiruchirappalli, India.

He has been working in the area of renewable energy applications since 2014.

**Subramaniam Senthilkumar** (M'17) received the B.E. degree in electrical and electronics engineering from Madurai Kamaraj University, Madurai, India, in 1999, the M.Tech. degree in electrical drives and control from Pondicherry University, Puducherry, India, in 2005, and the Ph.D. degree in electrical engineering from the National Institute of Technology, Tiruchirappalli, India, in 2013.

He has 17 years of teaching experience at various engineering institutions. Since April 2006, he has been an Assistant Professor at the National Institute of Technology. He has extensively researched on self-excited induction generators for standalone and grid-connected applications. His current research interests include the development of new power converter topologies for renewable energy systems.

**Dipankar Biswas** received the B.Tech. degree in electrical and electronics engineering from Jalpaiguri Government Engineering College, Jalpaiguri, India, in 2014, and the M.Tech. degree in power electronics from the National Institute of Technology, Tiruchirappalli, India, in June 2016.

He has worked in the area of power converters for renewable energy systems. He is currently with Indian Oil Corporation Limited, New Delhi, India.

**M. Kaliamoorthy** received the Bachelor's degree in electrical and electronics engineering from the University of Madras, Chennai, India, in 1999, the Master's degree in electrical drives and control from Pondicherry University, Puducherry, India, in 2006, and the Ph.D. degree in grid-connected multilevel inverters from Anna University, Chennai, in 2015.

He has nearly 16 years of teaching experience. Since 2016, he has been an Associate Professor with the Department of Electrical and Electronics Engineering, Dr. Mahalingam College of Engineering and Technology, Pollachi, India. His research interests include multilevel inverters and power electronics for renewable energy systems.

Dr. Kaliamoorthy was a gold medalist in his postgraduate program with Pondicherry University for the academic year 2005–2006.